iScience

CellPress
OPEN ACCESS

Article

Targeted down-regulation of SRSF1 exerts anti-cancer activity in OSCC through impairing lysosomal function and autophagy

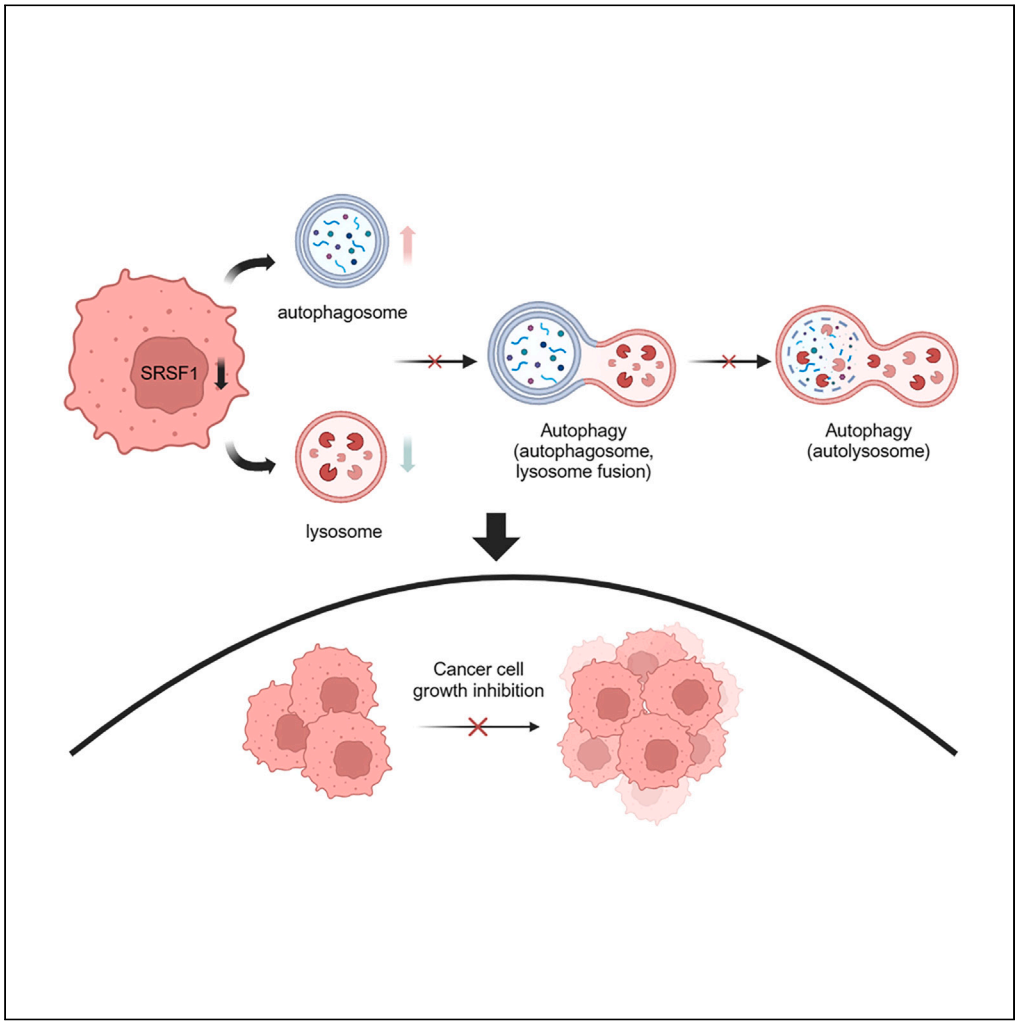

Yi Qu, Ying He, Yijuan Wang, Zhengxue Han, Lizheng Qin

zhengxue_han@163.com (Z.H.)
qinlizheng@ccmu.edu.cn (L.Q.)

Highlights

High expression of SRSF1 is associated with poor prognosis of OSCC patients

The growth of OSCC was significantly inhibited upon down-regulation of SRSF1

Targeted knockdown of SRSF1 impeded the process of lysosomal biosynthesis in OSCC

The impediment of lysosomal biogenesis obstructs the autophagic flux in OSCC

Qu et al., iScience *26*, 108330
December 15, 2023
https://doi.org/10.1016/j.isci.2023.108330

iScience

CellPress
OPEN ACCESS

Article

Targeted down-regulation of SRSF1 exerts anti-cancer activity in OSCC through impairing lysosomal function and autophagy

Yi Qu,[1] Ying He,[1] Yijuan Wang,[2] Zhengxue Han,[1,3,*] and Lizheng Qin[1,*]

SUMMARY

Oral squamous cell carcinoma (OSCC) is a common cancer of the head and neck. Despite ongoing efforts, there remains a dearth of targeted drugs capable of effectively inhibiting OSCC growth. As the earliest discovered proto-oncogene in the SRSF family, targeted inhibition of serine/arginine-rich splicing factor 1 (SRSF1) plays an important role in tumor suppression. However, the expression, function, and mechanism of SRSF1 in OSCC have not been comprehensively reported. This study retrospectively analyzed clinical samples from OSCC patients and discovered a significant correlation between the SRSF1 expression level and poor prognosis. *In vitro* experimentation demonstrated that SRSF1 knockdown inhibited OSCC growth, survival, lysosomal biogenesis and autophagy. To confirm the significance of lysosomal function and autophagy in the regulation of OSCC growth by SRSF1, cell rescue models were constructed. The aforementioned findings were subsequently validated in xenograft models. Ultimately, targeted knockdown of SRSF1 was found to significantly suppress OSCC growth by impeding lysosomal biogenesis and autophagy.

INTRODUCTION

Oral squamous cell carcinoma (OSCC) is among the most prevalent cancers, accounting for 1%–2% of all cancers.[1] Additionally, OSCC exhibits notable traits of elevated aggressiveness, frequent metastatic occurrences, and recurrent manifestations.[2] Therefore, the 5-year survival rate for patients with OSCC is nearly 50%.[3] The limited treatment options for OSCC can be attributed partly to the inadequate comprehension of its fundamental biology. The alternative splicing of pre-mRNA is one of the critical posttranslational processes determining the complexity of mammals' proteomes.[4] Dysregulation of splicing factors can lead to the failure to identify spice sites, ultimately resulting in the production of aberrant mature mRNA variants that encode harmful isoforms. This phenomenon is involved in the pathophysiology of cancer.[4,5]

Consequently, the "cancer" splicing factor is now considered a molecular biomarker as well as a therapeutic target to combat cancer.[6] The serine/arginine-rich splicing factors (SRSFs) constitute a significant protein family of splicing factors recently identified. They play a crucial role in the entire neoplastic genesis and progression process. It has been clarified that serine/arginine-rich splicing factor 1 (SRSF1), one of these SRSFs, has a direct function in tumorigenesis.[7] Increasing evidence demonstrates that SRSF1 exhibits elevated expression levels in various types of cancer and functions as an oncogene.[8–10] However, the contribution of SRSF1 to the onset and progression of OSCC has not yet been clearly elucidated. The lysosome is one of the most essential membrane-bound organelles in the catabolic process. The lysosomal microenvironment is composed of a variety of hydrolases that aid in the degradation of complex macromolecules such as large protein complexes, nucleotides, lipids, as well as glycoproteins. These processes are integral to endocytic receptor recycling and energy metabolism.[11] Maintenance of a homeostatic intracellular environment requires normal lysosomal biogenesis levels, while increased lysosomal biogenesis has been associated with rapid tumor growth and poor prognosis.[12] In addition, by regulating autophagy, lysosome-mediated signaling pathways, and transcription programs monitor cellular metabolism and switch between anabolism and catabolism, thereby affecting the rapid growth of tumor cells.[13,14]

Our research revealed that SRSF1 expression showed a significant increase in OSCC and that up-regulation of SRSF1 expression in tumor tissues predicted unfavorable patient outcomes. Furthermore, significant inhibition of rapid growth in OSCC was observed upon targeted knockdown of SRSF1, whereas overexpression of SRSF1 had the opposite effect. Through high-throughput RNA sequencing (RNA-seq) and subsequent *in vitro* and *in vivo* experimentation, it has been determined that suppression of lysosomal biogenesis and autophagy in OSCC cells can be achieved by knockdown of SRSF1. In turn, this has been shown to effectively impede tumor growth. This provides a new mechanism and evidence for targeting SRSF1 in treating OSCC.

[1]Department of Oral and Maxillofacial & Head and Neck Oncology, Beijing Stomatological Hospital, Capital Medical University, Beijing 100050, China
[2]Xiamen Key Laboratory of Stomatological Disease Diagnosis and Treatment Department of Oral and Maxillofacial Surgery, Stomatological Hospital of Xiamen Medical College, Xiamen, Fujian 361000, China
[3]Lead contact
*Correspondence: zhengxue_han@163.com (Z.H.), qinlizheng@ccmu.edu.cn (L.Q.)
https://doi.org/10.1016/j.isci.2023.108330

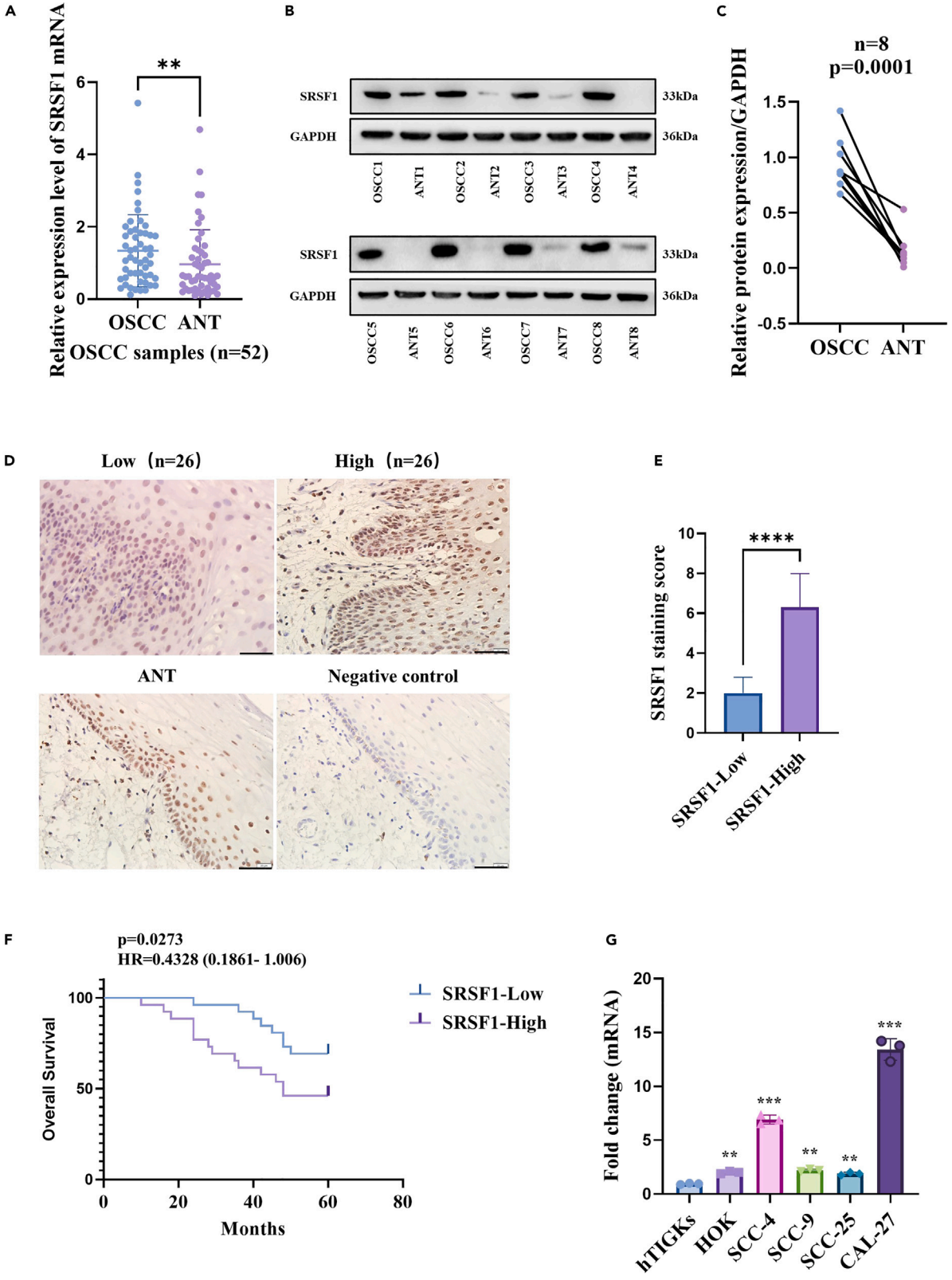
A
Relative expression level of SRSF1 mRNA
**
OSCC ANT
OSCC samples (n=52)
B
SRSF1
GAPDH
33kDa
36kDa
OSCC1 ANT1 OSCC2 ANT2 OSCC3 ANT3 OSCC4 ANT4
OSCC5 ANT5 OSCC6 ANT6 OSCC7 ANT7 OSCC8 ANT8
C
n=8
p=0.0001
Relative protein expression/GAPDH
OSCC ANT
D
Low (n=26)
High (n=26)
ANT
Negative control
E
SRSF1 staining score
****
SRSF1-Low
SRSF1-High
F
p=0.0273
HR=0.4328 (0.1861- 1.006)
Overall Survival
Months
SRSF1-Low
SRSF1-High
G
Fold change (mRNA)
hTIGKs HOK SCC-4 SCC-9 SCC-25 CAL-27

Figure 1. SRSF1 expression in OSCC tissues and cell lines

(A) RT-qPCR analysis of SRSF1 expression in 52 pairs of OSCC and ANTs.

(B and C) Representation of SRSF1 protein expression data in eight paired OSCC tissues and ANTs were identified utilizing western blot analysis.

(D) IHC staining of SRSF1 in control tissues (ANTs) and OSCC. The establishment of negative control was achieved through the utilization of PBS as a surrogate for the primary antibody. Scale bar: 50 μm.

(E) IHC staining score of SRSF1 in 52 cases of OSCC tissues.

(F) Kaplan-Meier survival analysis was performed to assess the correlation of SRSF1 expression in cancer tissues with OS of patients diagnosed with OSCC.

(G) SRSF1 mRNA expression in hTIGKS, HOK, and OSCC cell lines includes SCC-4, SCC-9, and SCC-25 in addition to CAL-27. Error bars express mean ± SD. **p < 0.01, ***p < 0.001, ****p < 0.0001.

RESULTS

SRSF1 is increased in OSCC patients and cell lines, and its higher expression estimates the poorer outcome

In order to establish SRSF1's function in OSCC, SRSF1 expression was assessed in 52 paired OSCC and adjacent normal tissues (ANTs) samples through RT-qPCR assay and western blot analysis. Compared to ANTs, the SRSF1 mRNA expression patterns significantly elevated OSCC tissues (p = 0.0034) (Figure 1A). Furthermore, the expression of the SRSF1 protein was consistent with the corresponding mRNA observations (Figures 1B and 1C). According to IHC staining, SRSF1 is primarily localized in the nucleus and strongly expressed in almost all OSCC tissues, while SRSF1 expression is weak or even negative in most ANTs (Figures 1D and 1E). Subsequently, the correlation between the SRSF1 expression pattern in cancer tissues and the clinical pathological criteria of patients with OSCC was analyzed. Table 1 lists the correlation of SRSF1 expression with a wide variety of clinicopathological characteristics. The results showed that the high-SRSF1 groups were obviously related to the clinical stages T3/T4 (p = 0.0054), advanced pathological grade (p = 0.0385), and high Ki-67 positive rates (p < 0.001). In the Kaplan-Meier analysis, high expression of SRSF1 was associated with a significant reduction in overall survival (OS) (p = 0.0273) compared to low expressions (Figure 1F). For the low SRSF1 groups, the OS measure was 69.2%, while for the high SRSF1 groups, the OS measure was 46.2%.

Then, we tested SRSF1 expression in two oral epithelial cell lines (hTIGKs and HOK) and four human OSCC cell lines (SCC-4, SCC-9, SCC-25, and CAL-27). Compared to human immortal gingival epithelial cells hTIGKs and human oral mucosa keratinocytes HOK, OSCC cells have significantly higher SRSF1 levels (Figure 1G). Furthermore, the expression patterns of SRSF1 were higher in the SCC-4 and CAL-27 cell lines than in the SCC-9 and SCC-25 cell lines.

Table 1. Relationship between SRSF1 protein expression and clinicopathological characteristics of the 52 OSCC patients

		SRSF1		
Variables	All cases	Low	High	p value[b]
Age[a]				0.7814
<63	25	13	12	
≥63	27	13	14	
Gender				0.3965
Male	31	14	17	
Female	21	12	9	
Clinical T stage				0.0054**
T1/T2	28	19	9	
T3/T4	24	7	17	
Pathological grade				0.0385*
I	11	9	2	
II/III	41	17	24	
Lymph node metastasis				>0.9999
Absent	30	15	15	
Present	22	11	11	
Ki-67[c]				<0.001***
≤60%	27	21	6	
>60%	25	5	20	

*p < 0.05, **p < 0.01, ***p < 0.001.

[a]63 years is the median age of the subjects.

[b]Chi-square test or Fisher's exact test.

[c]Percentage of ki-67 positive cells, 60% is the median value of the subjects.

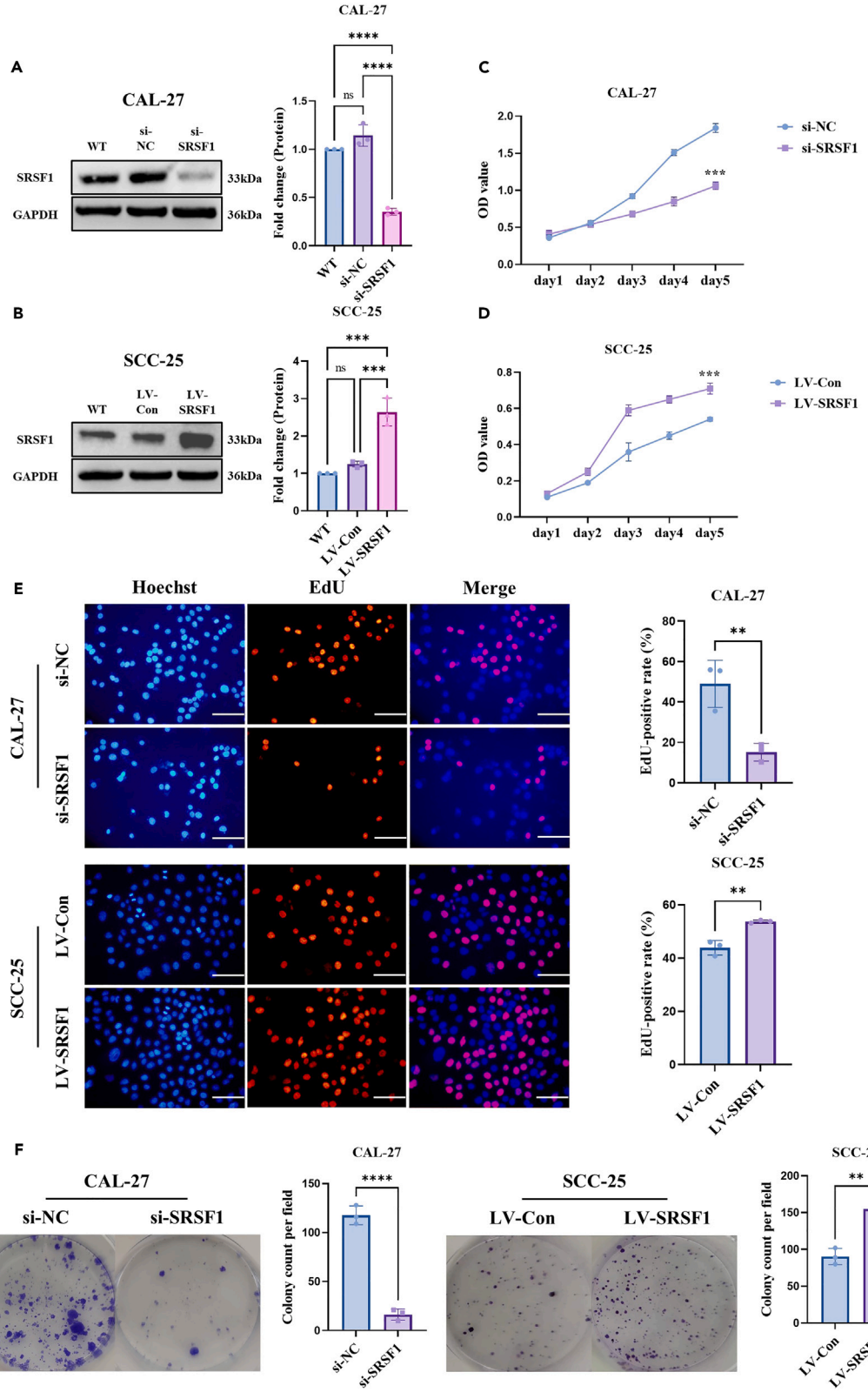
A
CAL-27
WT
si-NC
si-SRSF1
SRSF1
GAPDH
33kDa
36kDa
Fold change (Protein)
ns
****
B
SCC-25
LV-Con
LV-SRSF1
***
C
CAL-27
OD value
day1
day2
day3
day4
day5
si-NC
si-SRSF1
D
SCC-25
LV-Con
LV-SRSF1
E
Hoechst
EdU
Merge
EdU-positive rate (%)
**
F
Colony count per field

Figure 2. Down-regulation of SRSF1 suppressed the growth, proliferation, and colony-forming capacity of OSCC cells

(A and B) Western blot analysis of SRSF1 knockdown and up-regulation of CAL-27 and SCC-25 transfected with the lentivirus compared to the control lentivirus.

(C and D) Down-regulation of SRSF1 inhibited CAL-27 growth, while up-regulation of SRSF1 promoted SCC-25 growth.

(E) EdU staining was performed on OSCC cells. The figures presented represent customary illustrations of cell nuclei undergoing proliferation, stained with EdU (red) and Hoechst (blue). Additionally, combined images are included. Scale bar: 100 μm.

(F) The colony formation assay showed that reducing SRSF1 hindered OSCC survival while increasing SRSF1 had the opposite effect. The data were validated through duplicate trials. Error bars express mean ± SD. **p < 0.01, ***p < 0.001, ****p < 0.0001.

Targeted knockdown of SRSF1 blocked the growth and survival of OSCC

Motivated by the aforementioned discoveries, we investigated the role of SRSF1 in OSCC. CAL-27 and SCC-4 were used for stable knockdown of SRSF1, and SCC-25 and SCC-9 were used for overexpression of SRSF1. SRSF1 expression levels were confirmed using western blot (Figures 2A, 2B, S1A, and S1B). The SRSF1 knockdown effectiveness in si-SRSF1 CAL-27 and SCC-4 cells was 69.3% and 42.2%, respectively, and the SRSF1 overexpression efficiency in LV-SRSF1 SCC-25 and SCC-9 cells was 1.74-fold and 2.41-fold, respectively. To reflect the growth of OSCC cells more comprehensively, the study employed CCK-8 and EdU staining techniques to identify the collective and individual cellular growth of distinct groups. Based on the results, we found that the down-regulation of the target gene in CAL-27 and SCC-4 significantly inhibited cell growth and proliferation (Figures 2C, 2E, and S1C). However, up-regulation of SRSF1 in SCC-25 and SCC-9 enhanced cell growth and proliferation (Figures 2D, 2E, and S1D). The findings of the colony formation assay demonstrated that reducing SRSF1 expression impeded the viability of OSCC, whereas the augmentation of SRSF1 expression elicited a contrary outcome (Figures 2F, S1E and S1F).

SRSF1 has a role in the regulation of lysosomal-related pathways in OSCC

RNA-seq was applied to the si-NC and si-SRSF1 sub-cell lines of SCC-4 and CAL-27 to elucidate the potential mechanism of SRSF1's involvement in controlling the proliferation of OSCC. A total of 3,748 and 8,906 differentially expressed genes (DEGs) regulated with SRSF1 were identified in SCC-4 and CAL-27 cells, compared to the si-NC groups, 1,819 and 4,238 genes had decreased expression in SCC-4 and CAL-27, while 1,929 and 4,668 genes had elevated expression, respectively (Figures 3A and 3B).

According to the analysis of these DEGs in the Kyoto Encyclopedia of Genes and Genomes (KEGG), lysosomal-associated pathways were significantly inhibited in both cell lines after SRSF1 knockdown (Figures 3C and 3D). These differential genes related to lysosomal metabolism were mainly ATP subunit genes, fusion genes, lysosomal membrane protein genes, and protease genes, suggesting that SRSF1 may be involved in the regulation of lysosome biogenesis and lysosomal enzyme activity in OSCC (Figures 3E and 3F).

Targeted knockdown of SRSF1 inhibits lysosomal biogenesis and enzyme activity

Subsequently, we performed qRT-PCR on genes related to the lysosomal pathway in Figures 3E and 3F, and the results were aligned with the RNA-Seq analysis. In SCC-4 and CAL-27 cells, the mRNA expression patterns of GAA, ABCA2, LAMP3, MAN2B1, TCIRG1, SCARB2, GGA1, NAGLU, CTSZ, and M6PR showed a significant reduction compared to the control group (Figures 4A and 4B). To explore the impact of SRSF1 on the lysosomal role, the activity of the CTSD and NAGLU lysosomal enzymes was determined in si-NC and si-SRSF1 sub-cell lines. Significantly reduced activity of both enzymes was observed in si-SRSF1 groups (Figures 4C and 4D), confirming a general decline in the lysosomal role. OSCC cells were analyzed using LysoTracker red (DND-99) to determine the quantity and morphology of viable lysosomes. Compared to control cells, the count of lysosomes in the cytoplasm and fluorescence intensity decreased in si-SRSF1 transfected cells (Figures 4E and 4F). Moreover, no statistically significant variation in lysosomal morphology was observed among any group. Lysosomal-associated membrane protein 1 (LAMP1), a membrane protein regarded as a lysosomal marker,[15] is used to evaluate the count of intracellular lysosomes. According to western blot results, LAMP1, NAGLU, and CTSD protein expression patterns were significantly reduced after SRSF1 was knocked down in both SCC-4 and CAL-27 cell lines (Figures 4G, S2A and S2B).

TFEB is a crucial transcription factor that promotes lysosomal biogenesis. To confirm the crucial role of lysosomal biogenesis in SRSF1 regulating OSCC growth, we constructed a cell rescue model by transfection of si-SRSF1 sub-cell lines with TFEB plasmid. Western blot was utilized to determine the effectiveness of transfection (Figures 4H, S2C, and S2D). Figures 4I, 4J, S2E, and S2F show that up-regulation of TFEB significantly reversed the inhibitory impact of SRSF1 knockdown on cell growth, proliferation, and cloning.

The decrease in SRSF1 inhibits autophagic flux at its late stage

The biogenesis and functional impairment of lysosomes usually affect the normal autophagy process of tumor cells.[16] By analyzing the RNA-seq data, we found that many genes involved in the autophagy pathway, including ABL2, MAP1LC3B, NEDD4, CHMP2B, and LGALS8 were significantly activated after SRSF1 knockdown in OSCC (Figure 5A). Subsequently, the results of RNA-seq were further verified by RT-qPCR (Figures 5B and 5C). We tested changes in LC3B conversion by western blotting to explore the impact of SRSF1 on autophagy, and the LC3B-II protein accumulated markedly in si-SRSF1 groups. Furthermore, p62 was increased, consistent with the RNA-Seq analysis (Figures 5D, S3A, and S3B). Then, autophagic flux was assessed by transfection of cells with Ad-mCherry-GFP-LC3. This approach enables the emission of both mCherry and GFP signals upon targeting autophagosomes while only emitting the mCherry signal in autolysosomes due to quenching of GFP in the acidic lysosomal environment.[17] The findings shown in Figures 5E–5H indicate that the number of autophagosomes in both SCC-4 and CAL-27 cells increased significantly (yellow dots), and the number of autolysosomes decreased (red dots) after SRSF1 knockdown.

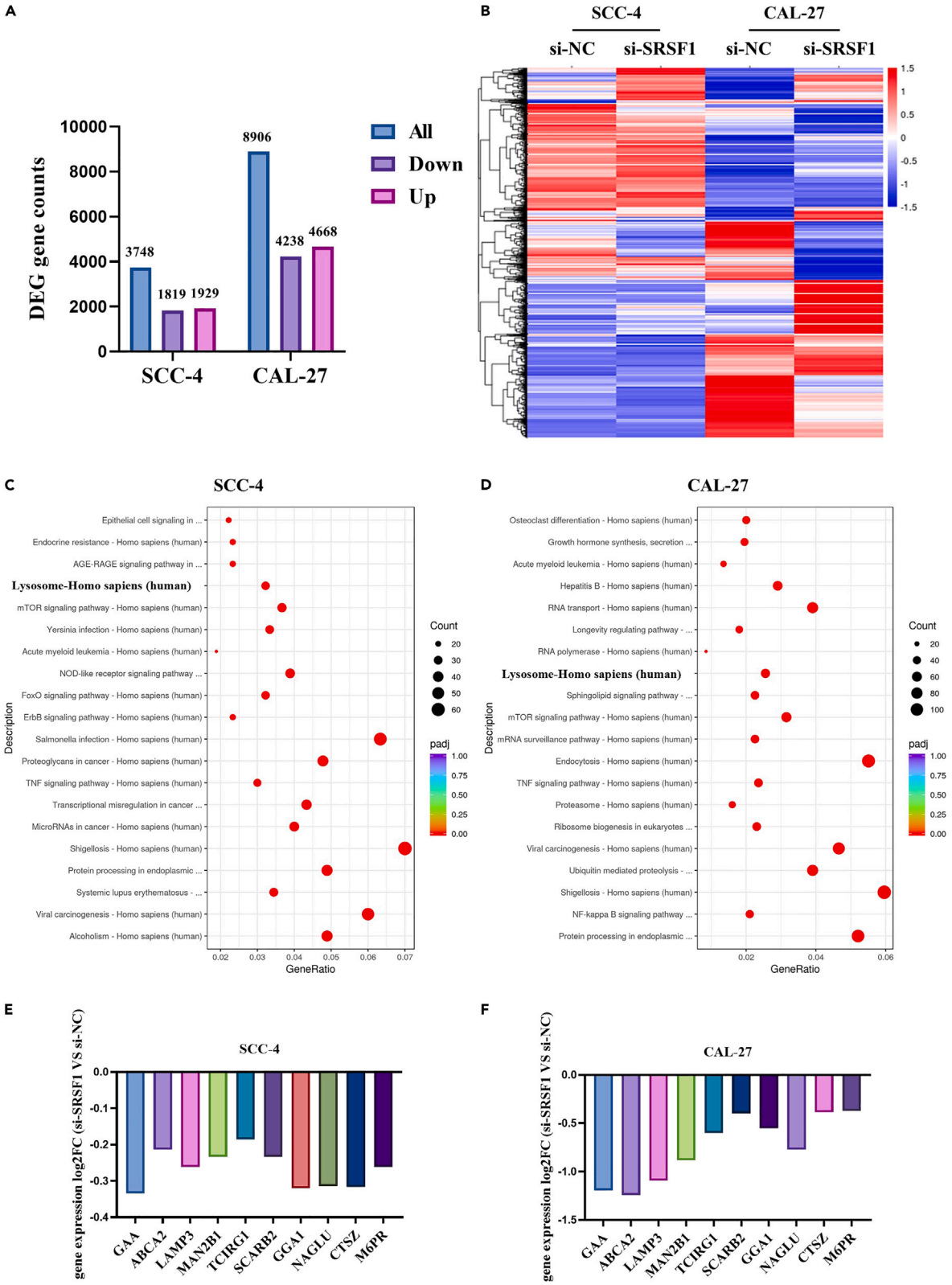
A
DEG gene counts
10000
8000
6000
4000
2000
0
3748
1819
1929
8906
4238
4668
SCC-4
CAL-27
All
Down
Up
B
SCC-4
CAL-27
si-NC
si-SRSF1
si-NC
si-SRSF1
1.5
1
0.5
0
-0.5
-1
-1.5
C
SCC-4
Epithelial cell signaling in ...
Endocrine resistance - Homo sapiens (human)
AGE-RAGE signaling pathway in ...
Lysosome-Homo sapiens (human)
mTOR signaling pathway - Homo sapiens (human)
Yersinia infection - Homo sapiens (human)
Acute myeloid leukemia - Homo sapiens (human)
NOD-like receptor signaling pathway ...
FoxO signaling pathway - Homo sapiens (human)
ErbB signaling pathway - Homo sapiens (human)
Salmonella infection - Homo sapiens (human)
Proteoglycans in cancer - Homo sapiens (human)
TNF signaling pathway - Homo sapiens (human)
Transcriptional misregulation in cancer ...
MicroRNAs in cancer - Homo sapiens (human)
Shigellosis - Homo sapiens (human)
Protein processing in endoplasmic ...
Systemic lupus erythematosus - ...
Viral carcinogenesis - Homo sapiens (human)
Alcoholism - Homo sapiens (human)
Description
0.02
0.03
0.04
0.05
0.06
0.07
GeneRatio
Count
20
30
40
50
60
padj
1.00
0.75
0.50
0.25
0.00
D
CAL-27
Osteoclast differentiation - Homo sapiens (human)
Growth hormone synthesis, secretion ...
Acute myeloid leukemia - Homo sapiens (human)
Hepatitis B - Homo sapiens (human)
RNA transport - Homo sapiens (human)
Longevity regulating pathway - ...
RNA polymerase - Homo sapiens (human)
Lysosome-Homo sapiens (human)
Sphingolipid signaling pathway - ...
mTOR signaling pathway - Homo sapiens (human)
mRNA surveillance pathway - Homo sapiens (human)
Endocytosis - Homo sapiens (human)
TNF signaling pathway - Homo sapiens (human)
Proteasome - Homo sapiens (human)
Ribosome biogenesis in eukaryotes ...
Viral carcinogenesis - Homo sapiens (human)
Ubiquitin mediated proteolysis - ...
Shigellosis - Homo sapiens (human)
NF-kappa B signaling pathway ...
Protein processing in endoplasmic ...
Description
0.02
0.04
0.06
GeneRatio
Count
20
40
60
80
100
padj
1.00
0.75
0.50
0.25
0.00
E
SCC-4
gene expression log2FC (si-SRSF1 VS si-NC)
0.0
-0.1
-0.2
-0.3
-0.4
GAA
ABCA2
LAMP3
MAN2B1
TCIRG1
SCARB2
GGA1
NAGLU
CTSZ
M6PR
F
CAL-27
gene expression log2FC (si-SRSF1 VS si-NC)
0.0
-0.5
-1.0
-1.5
GAA
ABCA2
LAMP3
MAN2B1
TCIRG1
SCARB2
GGA1
NAGLU
CTSZ
M6PR

Figure 3. RNA-seq analysis in SRSF1 knockdown SCC4 and CAL-27 cell lines

(A) Schematic representation of the quantity of differentially expressed genes (DEGs).

(B) The DEGs transcription heatmap in SCC-4 and CAL-27 after SRSF1 knockdown.

(C and D) KEGG pathway analysis showed that the same DEGs were enriched in lysosomal-related pathways after SRSF1 knockdown in both cell lines.

(E and F) Ten representative differential genes related to the lysosome were significantly regulated after SRSF1 knockdown in RNA-seq data.

Next, we used autophagy inhibitor Baf A1 (bafilomycin A1), which inhibits the fusion between autophagosomes and lysosomes, to evaluate the effect of SRSF1 knockdown on autophagic flux. The results demonstrated that down-regulation of SRSF1 further promoted the conversion of LC3B I to II with treatment of 50 nM Baf A1 (Figure S3D). Finally, we used immunofluorescence to detect changes in the co-localization of LC3 and LAMP1 after SRSF1 knockdown. As shown in Figure S3C, LC3 fluorescence intensity was increased, LAMP1 fluorescence intensity was decreased, but the co-localization of LC3 and LAMP1 did not change significantly. The aforementioned results indicated that although the down-regulation of SRSF1 can promote the formation of autophagosome, the lysosome damage caused by SRSF1 knockdown ultimately inhibits the formation of autolysosome and impedes the autophagic flux.

Down-regulation of SRSF1 suppressed xenograft tumorigenesis in OSCC

In order to conduct *in vivo* experiments, sub-cellular lines that were stable for OSCC were introduced into nude mice via injection. The xenografts belonging to the si-SRSF1 groups demonstrated decreased levels of SRSF1, while the LV-SRSF1 groups exhibited elevated SRSF1 patterns than the control groups (Figure 6G, S4C, and S4D). The findings of the study suggest that the injection of SRSF1-knockdown CAL-27 cells in mice resulted in a decrease in tumor volume, mass, and cell growth (as measured via Ki-67 index) in comparison to the si-NC group (Figures 6A, 6C, 6E, 6G, and S4A). On the contrary, in the up-regulation group of SRSF1, tumor volume, mass, and cell proliferation were promoted (Figures 6B, 6D, 6F, 6G, and S4B). The results of the IHC stain indicated that the down-expression of SRSF1 inhibited LAMP1 expression and promoted the expression of p62, while the up-regulation of SRSF1 had the opposite effect (Figures 6G, S4C, and S4D). In addition, we also used western blotting to detect the expression of p62 and LC3B II in tumor tissues of nude mice after the down-regulation of SRSF1, and the results were consistent with *in vitro* experiments (Figure S4E). The current *in vitro* and *in vivo* findings declared that the targeted reduction of SRSF1 can effectively suppress lysosomal biogenesis and function, inhibit cancer cell autophagy, and hinder the rapid growth of OSCC.

DISCUSSION

SRSF1 is a prototypical member of the SR protein family, documented in various malignancies and associated with unfavorable clinical outcomes. In breast cancer, SRSF1 was overexpressed in tumor tissues and positively related to clinical severity as well as poor prognosis.[7] Furthermore, up-regulation of SRSF1 exhibited a strong association with advanced age, advanced grade, increased Ki-67 index, and reduced OS in patients with glioma.[8] However, in OSCC, only a few studies indicated the up-regulation of SRSF1 in cancer tissues, but the link between SRSF1 expression and clinicopathological variables is still obscure.[18] Herein, we further confirm that SRSF1 expression was elevated in most OSCC tissues.

Furthermore, elevated expression of SRSF1 in OSCC is associated with greater malignancy of tumor phenotypes and an unfavorable prognosis. The results of this study indicate that SRSF1 may have promise as a predictive biomarker for people with OSCC. Recently, SRSF1 has been reported to be involved in a variety of biological processes in cancer cells, such as the control of alternative splicing, the control of translation, the transport of RNA, and the decay of RNA through nonsense-mediated mechanisms.[19,20] The targeted knockdown of SRSF1 as a therapeutic target could significantly inhibit tumor growth.[7,8] Jinji Ma et al. explored the role of SRSF1 in OSCC for the first time *in vitro* cell experiments and proposed that SRSF1 may play a role in enhancing the growth, invasiveness, and epithelial-mesenchymal transition of cell lines associated with OSCC.[21] Similarly, our *in vivo* and *in vitro* results confirmed that down-regulation of SRSF1 blocked OSCC cell growth, survival, and xenograft formation, while up-regulation of SRSF1 had the opposite effects.

To further investigate the potential mechanism underlying the regulation of OSCC growth by SRSF1, two OSCC cell lines exhibiting elevated SRSF1 expression were chosen. Subsequently, RNA-seq analysis was conducted to examine alterations in gene expression following SRSF1 knockdown in both cell lines. Interestingly, after the enrichment of common differential genes in SCC-4 and CAL-27 into the KEGG signaling pathways, the alteration of the lysosome-related pathways attracted our attention. Lysosomes are integral to several cellular activities, including macromolecular recycling, vesicle trafficking, metabolic reprogramming, and pro-growth signaling.[22] The accelerated growth of many cancer cells necessitates increased rates of vesicle trafficking, which is facilitated by exacerbated lysosome activity. This enables cellular material breakdown, clearance, and recycling to fulfill cell growth demands.[23] Therefore, targeting lysosomal biogenesis has gradually become a promising anti-cancer strategy for a variety of malignant tumors. This study demonstrated that down-regulation of SRSF1 significantly inhibited lysosome biogenesis and function in OSCC. The importance of lysosomal biogenesis in targeting SRSF1 for tumor growth inhibition was confirmed by transfection with the TFEB plasmid.

Autophagy is an essential mechanism for the breakdown of lysosomal cells that plays a significant role in both developmental processes and cancer development,[24] acting as a suppressor or promoter of tumor growth, depending on the specific circumstances and phases of cancer development. Some researchers have linked autophagy to the inhibition of OSCC progression; however, other studies have shown that autophagy is positively associated with the development and progression of OSCC.[25] Tang et al. reported that OSCC had a high degree of autophagy activity, and dual expression of tumor autophagy protein 5 (ATG5) and Beclin-1 (BECN1) expression served as a poor prognostic indicator for OSCC.[26] Zhang et al. confirmed that nuclear protein 1 (NUPR1) maintained autophagic flux and lysosomal functions by directly

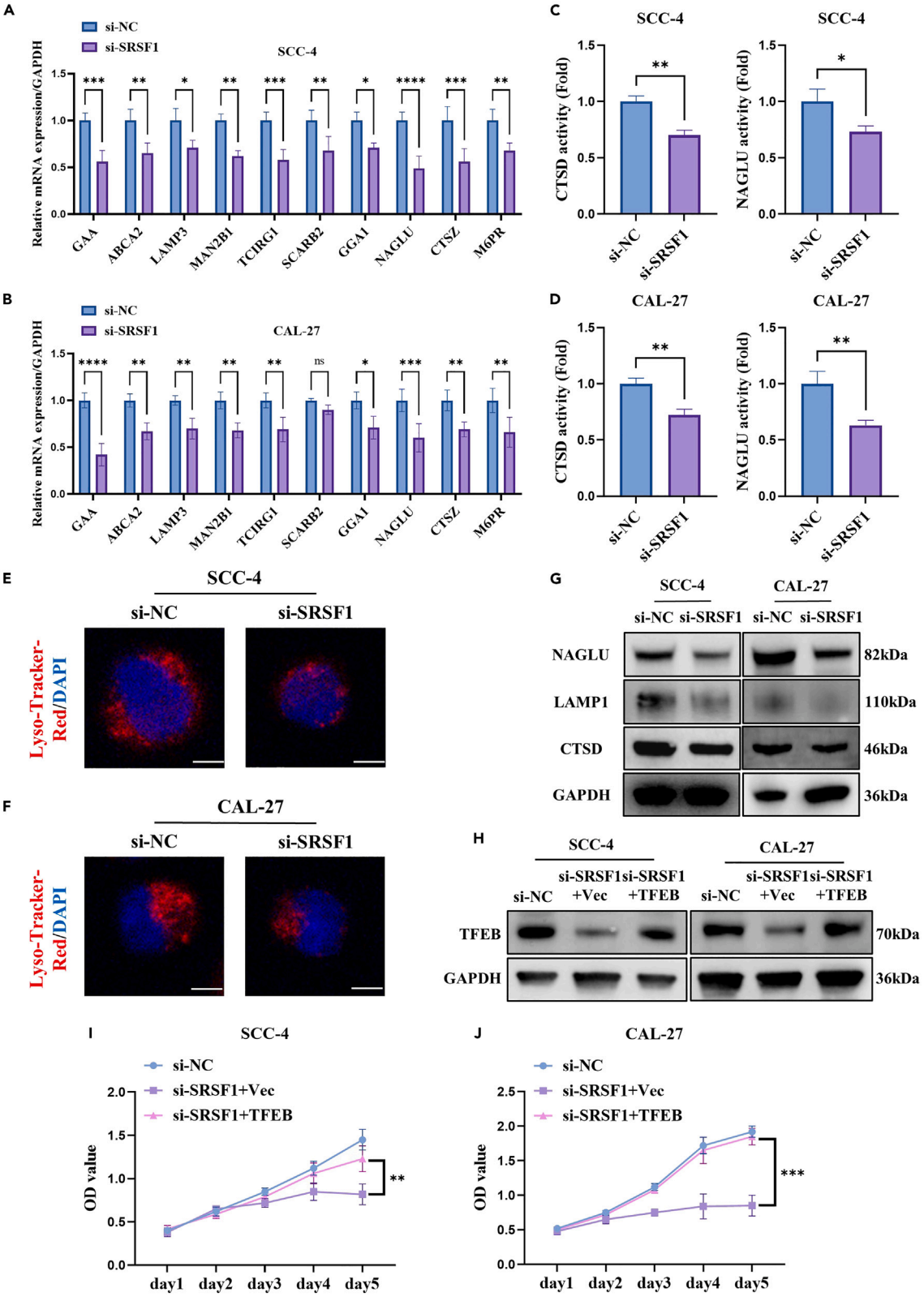
A
si-NC
si-SRSF1
SCC-4
Relative mRNA expression/GAPDH
GAA
ABCA2
LAMP3
MAN2B1
TCIRG1
SCARB2
GGA1
NAGLU
CTSZ
M6PR
B
CAL-27
C
SCC-4
CTSD activity (Fold)
NAGLU activity (Fold)
D
CAL-27
E
SCC-4
si-NC
si-SRSF1
Lyso-Tracker-Red/DAPI
F
CAL-27
G
SCC-4
CAL-27
NAGLU
LAMP1
CTSD
GAPDH
82kDa
110kDa
46kDa
36kDa
H
si-SRSF1+Vec
si-SRSF1+TFEB
TFEB
70kDa
I
SCC-4
si-SRSF1+Vec
si-SRSF1+TFEB
OD value
day1
day2
day3
day4
day5
J
CAL-27

Figure 4. Down-regulation of SRSF1 inhibited lysosomal biogenesis and function in OSCC

(A and B) The expression of ten genes related to lysosomal was detected by qRT-PCR in the si-NC and si-SRSF1 groups.

(C and D) The CTSD and NAGLU lysosomal enzyme activity was reduced after SRSF1 knockdown in both SCC-4 and CAL-27.

(E and F) OSCC cell lines were treated with a 50 nM LysoTracker red concentration for 30 min. Scale bar: 5 μm.

(G) Western blot technique was employed to identify the protein expression pattern of LAMP1, CTSD as well as NAGLU in both SCC-4 and CAL-27 after SRSF1 knockdown.

(H) Transfection of si-SRSF1 sub-cell lines with TFEB plasmid.

(I and J) CCK-8 assay showed that TFEB up-regulation showed a significant impact on alleviating the inhibitory impact of SRSF1 knockdown on the growth of OSCC cells. Error bars express mean ± SD. *$p < 0.05$, **$p < 0.01$, ***$p < 0.001$, ****$p < 0.0001$.

increasing transcription factor E3 (TFE3) activity, which promoted OSCC cell proliferation and metastasis *in vitro* and *in vivo*, based on tandem mass tag-based quantitative proteomic analysis.[27] Overexpression of miR-10b was followed by enhanced OSCC invasion and migration and activated autophagic protein, such as LC3II/ATG5. Through *in vivo* and *in vitro* experiments, we confirmed that in OSCC, the down-regulation of SRSF1 played a role in promoting autophagosome formation, which was consistent with previous findings in lung cancer.[28] However, SRSF1 knockdown also impaired lysosomal biogenesis and function, hindering autolysosome formation and ultimately suppressing autophagic flux.

In summary, the data presented in this study offer important information on the function and fundamental mechanisms of aberrant regulation of SRSF1 in OSCC. This research indicated that down-regulation of SRSF1 suppresses tumor growth and survival by inhibiting lysosomal function and autophagy. Furthermore, our research found a significant positive link between SRSF1 expression and clinical T stage, pathological grade, Ki-67 index, and poor survival in patients with OSCC. Based on the collective findings of these investigations, we suggest that SRSF1 has the capacity to serve as both a predictive indicator and a significant anti-cancer therapeutic target, with the possibility of practical application in the context of OSCC.

Limitations of the study

However, it is still unclear which target gene pre-mRNA splicing is directly regulated by SRSF1 to inhibit the biogenesis and function of lysosomes in OSCC and the correlation between lysosomal and autophagy dysfunction caused by SRSF1 knockdown. The issues mentioned previously will constitute the primary focus of our subsequent investigation.

STAR★METHODS

Detailed methods are provided in the online version of this paper and include the following:

- KEY RESOURCES TABLE
- RESOURCE AVAILABILITY
  - Lead contact
  - Materials availability
  - Data and code availability
- EXPERIMENTAL MODEL AND STUDY PARTICIPANT DETAILS
  - Tissue samples and clinicopathological data
  - Animal experiments
  - Cell culture and reagents
- METHOD DETAILS
  - RNA extraction and qRT-PCR
  - Protein extraction and Western blot
  - Immunohistochemistry
  - Lentiviruses and plasmids
  - Assessment of cell growth, proliferation, and survival
  - RNA-seq and data analysis
  - Lysosomal enzyme assay
  - Lysosomal staining
  - Ad-mCherry-GFP-LC3 infection analysis
  - Immunofluorescence
- QUANTIFICATION AND STATISTICAL ANALYSIS

SUPPLEMENTAL INFORMATION

Supplemental information can be found online at https://doi.org/10.1016/j.isci.2023.108330.

ACKNOWLEDGMENTS

This research was supported by the Beijing Stomatological Hospital, Capital Medical University Young Scientist Program (NO. YSP202107).

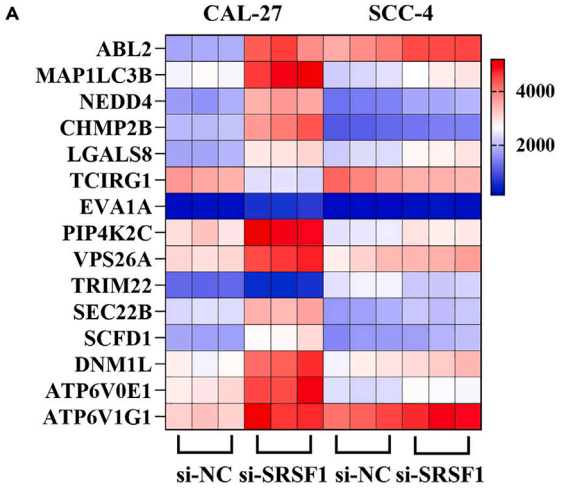
A
CAL-27
SCC-4
ABL2
MAP1LC3B
NEDD4
CHMP2B
LGALS8
TCIRG1
EVA1A
PIP4K2C
VPS26A
TRIM22
SEC22B
SCFD1
DNM1L
ATP6V0E1
ATP6V1G1
4000
2000
si-NC si-SRSF1 si-NC si-SRSF1

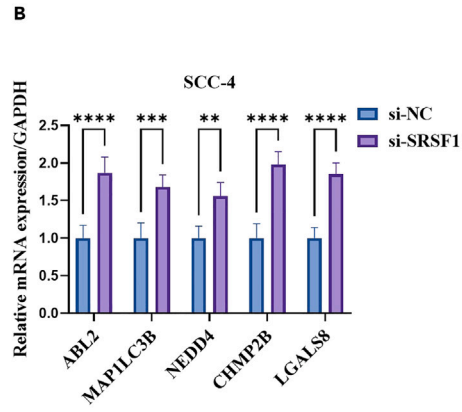
B
SCC-4
si-NC
si-SRSF1
Relative mRNA expression/GAPDH
ABL2
MAP1LC3B
NEDD4
CHMP2B
LGALS8

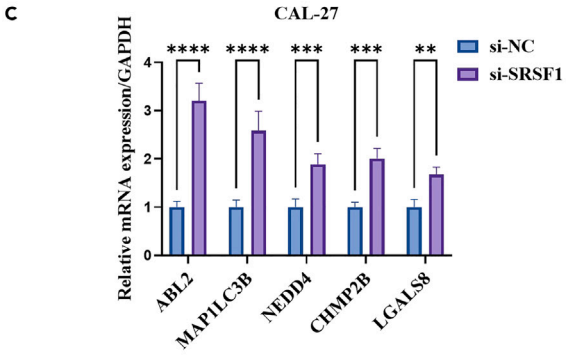
C
CAL-27
si-NC
si-SRSF1
Relative mRNA expression/GAPDH
ABL2
MAP1LC3B
NEDD4
CHMP2B
LGALS8

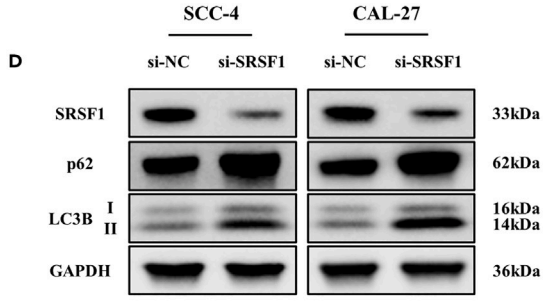
D
SCC-4
CAL-27
si-NC
si-SRSF1
si-NC
si-SRSF1
SRSF1
p62
LC3B
I
II
GAPDH
33kDa
62kDa
16kDa
14kDa
36kDa

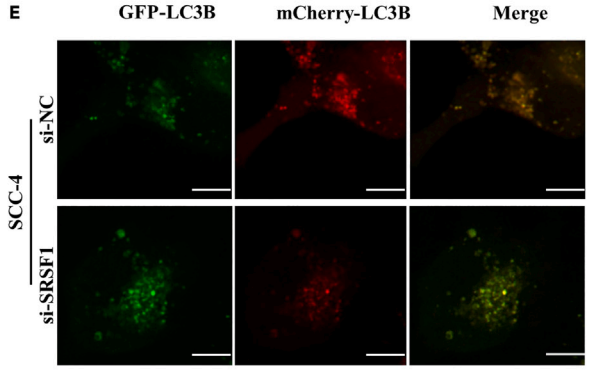
E
GFP-LC3B
mCherry-LC3B
Merge
SCC-4
si-NC
si-SRSF1

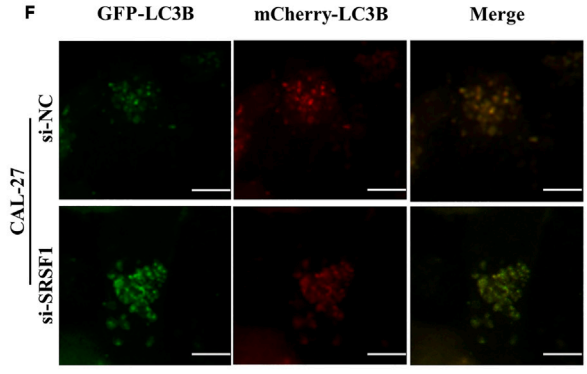
F
GFP-LC3B
mCherry-LC3B
Merge
CAL-27
si-NC
si-SRSF1

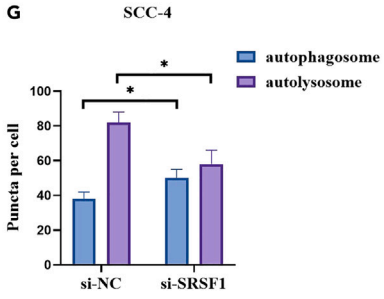
G
SCC-4
autophagosome
autolysosome
Puncta per cell
si-NC
si-SRSF1

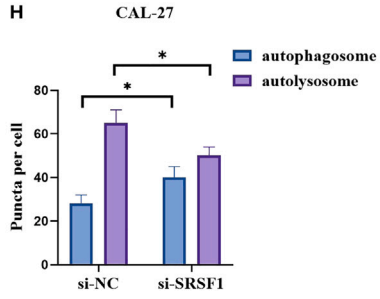
H
CAL-27
autophagosome
autolysosome
Puncta per cell
si-NC
si-SRSF1

Figure 5. Reduced SRSF1 is associated with decreased autophagy

(A) Heat maps of 15 representative autophagy-related differential genes after SRSF1 knockdown in SCC-4 and CAL-27 were derived from RNA-seq data.
(B and C) qRT-PCR was used to detect the mRNA expression levels of ABL2, MAP1LC3B, NEDD4, CHMP2B, and LGALS8 in different OSCC groups.
(D) The protein expression patterns of SRSF1, P62, and LC3B in various groups were identified utilizing western blot.
(E–H) SCC-4 and CAL-27 cells with stable down-regulation of SRSF1 were transfected with GFP-mCherry-LC3 to explore GFP expression and mCherry using a laser confocal microscope. Three experimental trials were conducted, and the average value, along with the SD of the count of autophagosomes (represented by yellow dots) and autolysosomes (represented by red-only dots) per cell, were graphed. Scale bar: 50 μm. Error bars express mean ± SD. *p < 0.05, **p < 0.01, ***p < 0.001, ****p < 0.0001.

AUTHOR CONTRIBUTIONS

L.Q. and Z.H.: Conceptualization, Methodology, Supervision, Project administration, Resources. Y.Q.: Investigation, Data curation, Writing-Original draft, Validation. Y.H. and Y.W.: Writing-Review & Editing, Visualization.

DECLARATION OF INTERESTS

The authors declare no competing interests.

INCLUSION AND DIVERSITY

We support inclusive, diverse, and equitable conduct of research.

Received: June 8, 2023
Revised: September 5, 2023
Accepted: October 20, 2023
Published: October 27, 2023

REFERENCES

1. Chai, A.W.Y., Lim, K.P., and Cheong, S.C. (2020). Translational genomics and recent advances in oral squamous cell carcinoma. Semin. Cancer Biol. *61*, 71–83.
2. Liu, J., Jiang, X., Zou, A., Mai, Z., Huang, Z., Sun, L., and Zhao, J. (2021). circIGHG-Induced Epithelial-to-Mesenchymal Transition Promotes Oral Squamous Cell Carcinoma Progression via miR-142-5p/IGF2BP3 Signaling. Cancer Res. *81*, 344–355.
3. Dong, Y., Xue, L., Zhang, Y., Liu, C., Zhang, Y., Jiang, N., Ma, X., Chen, F., Li, L., Yu, L., et al. (2022). Identification of RNA-splicing factor Lsm12 as a novel tumor-associated gene and a potent biomarker in Oral Squamous Cell Carcinoma (OSCC). J. Exp. Clin. Cancer Res. *41*, 150.
4. David, C.J., and Manley, J.L. (2010). Alternative pre-mRNA splicing regulation in cancer: pathways and programs unhinged. Genes Dev. *24*, 2343–2364.
5. Oltean, S., and Bates, D.O. (2014). Hallmarks of alternative splicing in cancer. Oncogene *33*, 5311–5318.
6. Liu, Z., Yoshimi, A., Wang, J., Cho, H., Chun-Wei Lee, S., Ki, M., Bitner, L., Chu, T., Shah, H., Liu, B., et al. (2020). Mutations in the RNA Splicing Factor SF3B1 Promote Tumorigenesis through MYC Stabilization. Cancer Discov. *10*, 806–821.
7. Du, J.X., Luo, Y.H., Zhang, S.J., Wang, B., Chen, C., Zhu, G.Q., Zhu, P., Cai, C.Z., Wan, J.L., Cai, J.L., et al. (2021). Splicing factor SRSF1 promotes breast cancer progression via oncogenic splice switching of PTPMT1. J. Exp. Clin. Cancer Res. *40*, 171.
8. Zhou, X., Wang, R., Li, X., Yu, L., Hua, D., Sun, C., Shi, C., Luo, W., Rao, C., Jiang, Z., et al. (2019). Splicing factor SRSF1 promotes gliomagenesis via oncogenic splice-switching of MYO1B. J. Clin. Invest. *129*, 676–693.
9. Mo, Y., Wang, Y., Wang, Y., Deng, X., Yan, Q., Fan, C., Zhang, S., Zhang, S., Gong, Z., Shi, L., et al. (2022). Circular RNA circPVT1 promotes nasopharyngeal carcinoma metastasis via the β-TrCP/c-Myc/SRSF1 positive feedback loop. Mol. Cancer *21*, 192.
10. Hall, A.E., Pohl, S.Ö.G., Cammareri, P., Aitken, S., Younger, N.T., Raponi, M., Billard, C.V., Carrancio, A.B., Bastem, A., Freile, P., et al. (2022). RNA splicing is a key mediator of tumour cell plasticity and a therapeutic vulnerability in colorectal cancer. Nat. Commun. *13*, 2791.
11. Shin, H.R., and Zoncu, R. (2020). The Lysosome at the Intersection of Cellular Growth and Destruction. Dev. Cell *54*, 226–238. https://doi.org/10.1016/j.devcel.2020.06.010.
12. Shin, H.R., and Zoncu, R. (2020). The Lysosome at the Intersection of Cellular Growth and Destruction. Dev. Cell *54*, 226–238.
13. Li, X., He, S., and Ma, B. (2020). Autophagy and autophagy-related proteins in cancer. Mol. Cancer *19*, 12.
14. Li, X., He, S., and Ma, B. (2020). Autophagy and autophagy-related proteins in cancer. Mol. Cancer *19*, 12.
15. Sharoar, M.G., Palko, S., Ge, Y., Saido, T.C., and Yan, R. (2021). Accumulation of saposin in dystrophic neurites is linked to impaired lysosomal functions in Alzheimer's disease brains. Mol. Neurodegener. *16*, 45.
16. Kroemer, G., and Jäättelä, M. (2005). Lysosomes and autophagy in cell death control. Nat. Rev. Cancer *5*, 886–897.
17. Yang, Y., Gao, J., Zhang, Y., Xu, W., Hao, Y., Xu, Z., and Tao, L. (2018). Natural pyrethrins induce autophagy of HepG2 cells through the activation of AMPK/mTOR pathway. Environ. Pollut. *241*, 1091–1097.
18. Xu, Z., Han, X., Tang, Z., Tian, G., Gao, J., and Xu, X. (2017). Interaction between MALAT-1, CCR7 and correlated genes in oral squamous cell carcinoma. Int. J. Clin. Exp. Pathol. *10*, 10730–10739.
19. Li, S., Qi, Y., Yu, J., Hao, Y., He, B., Zhang, M., Dai, Z., Jiang, T., Li, S., Huang, F., et al. (2022). Nuclear Aurora kinase A switches m6A reader YTHDC1 to enhance an oncogenic RNA splicing of tumor suppressor RBM4. Signal Transduct. Target. Ther. *7*, 97.
20. Liu, J., You, M., Yao, Y., Ji, C., Wang, Z., Wang, F., Wang, D., Qi, Z., Yu, G., Sun, Z., et al. (2021). SRSF1 plays a critical role in invariant natural killer T cell development and function. Cell. Mol. Immunol. *18*, 2502–2515.
21. Zhang, Y., Wang, A., Zhang, X., Wang, X., Zhang, J., and Ma, J. (2021). lncRNA LINC01296 Promotes Oral Squamous Cell Carcinoma Development by Binding with SRSF1. BioMed Res. Int. *2021*, 6661520.
22. Saftig, P., and Klumperman, J. (2009). Lysosome biogenesis and lysosomal membrane proteins: trafficking meets function. Nat. Rev. Mol. Cell Biol. *10*, 623–635.
23. Settembre, C., Fraldi, A., Medina, D.L., and Ballabio, A. (2013). Signals from the lysosome: a control centre for cellular clearance and energy metabolism. Nat. Rev. Mol. Cell Biol. *14*, 283–296.
24. Kondo, Y., Kanzawa, T., Sawaya, R., and Kondo, S. (2005). The role of autophagy in cancer development and response to therapy. Nat. Rev. Cancer *5*, 726–734.
25. White, E. (2012). Deconvoluting the context-dependent role for autophagy in cancer. Nat. Rev. Cancer *12*, 401–410.
26. Tang, J.Y., Fang, Y.Y., Hsi, E., Huang, Y.C., Hsu, N.C.H., Yang, W.C., Chang, H.W., Chai, C.Y., and Chu, P.Y. (2013). Immunopositivity of Beclin-1 and ATG5 as indicators of survival and disease recurrence in oral squamous cell carcinoma. Anticancer Res. *33*, 5611–5616.
27. Fan, T., Wang, X., Zhang, S., Deng, P., Jiang, Y., Liang, Y., Jie, S., Wang, Q., Li, C., Tian, G., et al. (2022). NUPR1 promotes the proliferation and metastasis of oral squamous cell carcinoma cells by activating TFE3-

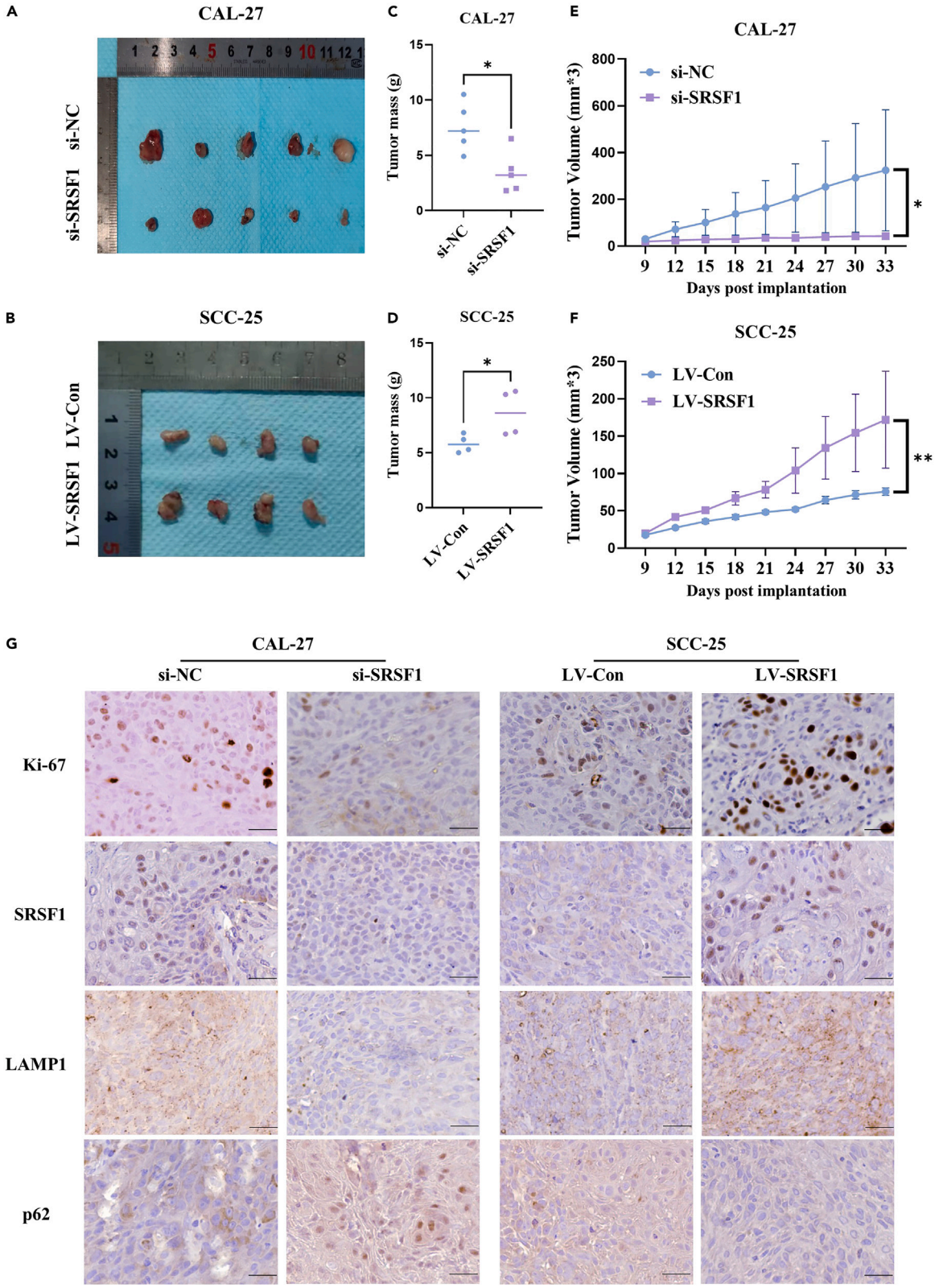
A
CAL-27
si-NC
si-SRSF1
B
SCC-25
LV-Con
LV-SRSF1
C
CAL-27
Tumor mass (g)
si-NC
si-SRSF1
D
SCC-25
Tumor mass (g)
LV-Con
LV-SRSF1
E
CAL-27
si-NC
si-SRSF1
Tumor Volume (mm*3)
Days post implantation
F
SCC-25
LV-Con
LV-SRSF1
Tumor Volume (mm*3)
Days post implantation
G
CAL-27
SCC-25
si-NC
si-SRSF1
LV-Con
LV-SRSF1
Ki-67
SRSF1
LAMP1
p62

Figure 6. The suppression of tumor development was observed in xenograft models after the down-regulation of SRSF1

(A–D) The size of the tumors xenografted in different groups of BALB/c nude mice was compared to reflect the effect of SRSF1 on OSCC tumorigenesis. (A and B) Demonstrate the tumor xenografts subsequent to ectopic-subcutaneous implantation in nude mice, with a duration of one month. (C and D) The tumor mass was observed and recorded.

(E and F) After tumor formation, tumor volume was measured and recorded every three days until mice were killed after one month.

(G) IHC staining of SRSF1, Ki-67, LAMP1, and p62 in the xenograft tumor samples. Scale bar: 20 μm. Error bars express mean ± SD. *p < 0.05, **p < 0.01.

dependent autophagy. Signal Transduct. Target. Ther. *7*, 130.

28. Lv, Y., Zhang, W., Zhao, J., Sun, B., Qi, Y., Ji, H., Chen, C., Zhang, J., Sheng, J., Wang, T., et al. (2021). SRSF1 inhibits autophagy through regulating Bcl-x splicing and interacting with PIK3C3 in lung cancer. Signal Transduct. Target. Ther. *6*, 108.
29. Qu, Y., He, Y., Ruan, H., Qin, L., and Han, Z. (2023). Abnormal downregulation of 10-formyltetrahydrofolate dehydrogenase promotes the progression of oral squamous cell carcinoma by activating PI3K/Akt/Rb pathway. Cancer Med. *12*, 5781–5797.
30. Qu, Y., He, Y., Yang, Y., Li, S., An, W., Li, Z., Wang, X., Han, Z., and Qin, L. (2020). ALDH3A1 acts as a prognostic biomarker and inhibits the epithelial mesenchymal transition of oral squamous cell carcinoma through IL-6/STAT3 signaling pathway. J. Cancer *11*, 2621–2631.
31. Cheng, Y., Shen, Z., Gao, Y., Chen, F., Xu, H., Mo, Q., Chu, X., Peng, C.L., McKenzie, T.T., Palacios, B.E., et al. (2022). Phase transition and remodeling complex assembly are important for SS18-SSX oncogenic activity in synovial sarcomas. Nat. Commun. *13*, 2724.

STAR★METHODS

KEY RESOURCES TABLE

REAGENT or RESOURCE	SOURCE	IDENTIFIER
Antibodies		
Mouse anti-human SRSF1	Santa curz	Cat#sc-33652
Mouse anti-human GAPDH	Abclonal	RRID:AB_2769570
Rabbit anti-human NAGLU	Abcam	Cat#ab214671
Rabbit anti-human LAMP1	Abcam	RRID:AB_775978
Mouse anti-human CTSD	Santa curz	Cat#sc-377299
Rabbit anti-human TFEB	Bioss	RRID:AB_10855158
Rabbit anti-human p62	Abcam	RRID:AB_2810880
Rabbit anti-human LC3B	Abclonal	RRID:AB_2862723
Rabbit anti-human Ki-67	Abcam	RRID:AB_443209
Goat Anti-Mouse IgG H&L (Alexa Fluor® 488)	Abcam	RRID:AB_2576208
ABflo® 594-conjugated Goat Anti-Rabbit IgG (H+L)	Abclonal	RRID:AB_2768326
Anti-rabbit IgG	Cell Signaling Technology	Cat#7074
Anti-mouse IgG	Cell Signaling Technology	Cat#7076
Bacterial and virus strains		
LV-GV248-SRSF1-Human	Genechem	N/A
LV-CV146-SRSF1-Human	Genechem	N/A
Chemicals, peptides, and recombinant proteins		
Bafilomycin A1	MedChemExpress	Cat#HY-100558
Critical commercial assays		
TRIzol Reagent	CWbiotech	Cat#CW0580
PrimeScript™ RT reagent Kit with gDNA Eraser	TaKaRa	Cat#RR047Q
QuantiTect SYBR Green PCR Kit	QIAGEN	Cat#204145
Tissue Protein Extraction Kit	CWbiotech	Cat#CW0891
Lipofectamine™ 3000	Invitrogen	Cat#L3000001
Cell Counting Kit-8	Beyotime	Cat#C0037
BeyoClick™ EdU Cell Proliferation Kit with Alexa Fluor 555	Beyotime	Cat#C0075S
Cathepsin D Activity Assay Kit	Biovision	Cat#K143-100
β-N-Acetylglucosaminidase Assay Kit	Sigma-Aldrich	Cat#CS0780
Lyso-Tracker Red	Beyotime	Cat#C1046
adenovirus expressing mCherry-GFP-LC3B fusion protein	Beyotime	Cat#C3011
Deposited data		
RNAseq Data	This paper	GSE244710
Experimental models: Cell lines		
SCC-4	ATCC	CRL-1624
SCC-9	ATCC	CRL-1629
SCC-25	ATCC	CRL-1628
CAL-27	ATCC	CRL-2095
hTIGKs	ATCC	CRL-3397

(*Continued on next page*)

Continued

REAGENT or RESOURCE	SOURCE	IDENTIFIER
HOK	Shanxi Medical University School and Hospital of Stomatology	N/A
Experimental models: Organisms/strains		
BALB/c nude mice	Beijing HFK Bioscience	N/A
Oligonucleotides		
See Table S1	Life Technologies	N/A
Recombinant DNA		
Plasmid- GV740-TFEB-Human	Genechem	N/A
Software and algorithms		
SPSS V19.0 software	IBM	https://www.ibm.com/spss
Prism 9.4.1 software	GraphPad	https://www.graphpad.com/features
ImageJ	NIH	https://imagej.nih.gov/ij/

RESOURCE AVAILABILITY

Lead contact

Additional information and requests for resources and reagents should be directed to, and will be fulfilled by, the lead contact, Dr. Zhengxue Han (Zhengxue_Han@163.com).

Materials availability

This study did not generate new unique reagents.

Data and code availability

- RNA sequencing data is publicly available through Gene Expression Omnibus (GSE244710).
- This paper does not report original code.
- Any additional information required to reanalyze the data reported in this paper is available from the lead contact upon request.

EXPERIMENTAL MODEL AND STUDY PARTICIPANT DETAILS

Tissue samples and clinicopathological data

From January 2015 to January 2017, 52 patients included in this cohort study had primary OSCC confirmed by histopathology and were admitted to Beijing Stomatology Hospital, Capital Medical University. Neither radiotherapy nor chemotherapy had been administered previously to any patient. Every three months, data on subjects' initial state and subsequent clinical progress were gathered and periodically modified. Based on AJCC and WHO guidelines, tumor staging and grading were performed. Postoperative follow-up was initiated after the date of surgery and persisted until the patient's death or the completion of the monitoring. Following surgical resection, samples of OSCC and adjacent normal tissues (ANTs) were promptly partitioned into two segments. The initial segment was promptly cryopreserved and maintained at -80 °C for subsequent evaluation by Western blotting and quantitative reverse transcription-PCR (qRT-PCR) methods.

In contrast, the second part was fixed with 4% paraformaldehyde for immunohistochemistry (IHC) staining. As mentioned above, the collection of samples and data was conducted in accordance with the Helsinki Declaration. Consent was obtained from all patients and the Research Ethics Committee of the Beijing Stomatology Hospital to conduct the investigation.

Animal experiments

The Institutional Research Ethics Committee of the Stomatology Hospital of Capital Medical University approved the animal experiments. Beijing HFK Bioscience (China) provided female BALB/c nude mice (four weeks old) for each group at random. To examine the progression of tumors, a collection of sub-cell lines that had been infected with lentiviruses and subsequently chosen through puromycin selection were transplanted subcutaneously into mice. The transplantation was carried out by administering 1×10^6 cells per mouse, either on the left or right flank. Digital Vernier calipers were used to measure each tumor's length (L) and width (W) every three days after it formed. Tumor volumes were calculated by the following, Tumor volume $=W^2\times L/2$. Mice were anesthetized and killed a month after tumor formation. The initial neoplastic growths were excised, subsequently preserved, and then incorporated into paraffin for IHC staining.

Cell culture and reagents

The American Type Culture Collection (ATCC) provided hTIGKs, SCC-4, SCC-9, SCC-25, and CAL-27 cells. Shanxi Medical University School and Hospital of Stomatology supplied HOK cells. CAL-27 cells were grown in DMEM with 10% FBS and 0.5% penicillin/streptomycin. hTIGK cells were cultured in a dermal cell basal medium enriched with the Keratinocyte Growth Kit. The SCC-4, SCC-9, and SCC-25 cell lines were also grown in DMEM/F12 medium enriched with 10% FBS, 0.5% penicillin-streptomycin, and 400 ng/mL hydrocortisone. The HOK cells were cultured utilizing the Keratinocyte SFM media. The cells were stored in a humidified incubator at 37 °C with a CO_2 concentration of 5%.

METHOD DETAILS

RNA extraction and qRT-PCR

Total RNA was extracted using TRIzol reagent (CWbiotech, China). Following an evaluation of the concentration and purity of RNA, cDNA was synthesized utilizing the PrimeScript RT Reagent Kit (Takara, Japan). The SYBR Green PCR kit (Qiagen, Germany) was used to perform qRT-PCR. The $2^{-\Delta\Delta Ct}$ approach was used to compare relative mRNA expressions normalized to GAPDH expression. Table S1 lists the sequence of primers created and supplied by Life Technologies (Shanghai, China).

Protein extraction and Western blot

A tissue protein extraction kit (CWbiotech) was used to extract total proteins. Lysates and immunoblotting were carried out, as mentioned earlier.[29] In brief, the samples were homogenized and incubated by shaking constantly followed by centrifugation. The western blot membrane (PVDF, Millipore) was incubated overnight at 4°C with a SRSF1 antibody (sc-33652, Santa Cruz Biotechnology, USA, dilution 1:200), a NAGLU antibody (ab214671, Abcam, dilution 1:1000), a LAMP1 antibody (ab24170, Abcam, dilution 1:1000), a CTSD antibody (sc-377299, Santa Cruz Biotechnology, USA, dilution 1:200), a TFEB antibody (bs-5137R, Bioss, dilution 1:2000), a p62 antibody (ab109012, Abcam, dilution 1:1000) and a LC3B antibody (A19665, Abclonal, dilution 1:2000) subsequently incubated for 1 h with secondary HRP-conjugated antibodies, and finally incubated in Clarity Western ECL Substrate (BioRad, USA). Densitometric analysis was performed using ImageJ software. For the housekeeping gene, GAPDH antibody (AC033, Abclonal, dilution 1:100000) was used. Table S2 provides information on primary antibodies.

Immunohistochemistry

Paraffin-embedded tissue slides were dewaxed in xylene. Antigen retrieval was performed in citrate buffer at high temperature, followed by natural cooling to room temperature. Tissues were then blocked for 1 h, then incubated with the primary antibody against SRSF1 (sc-33652, Santa Cruz Biotechnology, USA, dilution 1:200), Ki-67 (ab15580, Abcam, dilution 1:200), LAMP1 (ab24170, Abcam, dilution 1:200), p62 (ab109012, Abcam, dilution 1:200), 4°C, overnight. The slides were then washed with PBST to remove unbound primary antibody, followed by incubation with goat anti-rabbit/mouse IgG/HRP polymer (Zsbio, Peking, China), for 25 min, at 37°C. Slides were then stained with DAB followed by counterstaining with hematoxylin. The tissues were dehydrated and sealed. The slides were scanned using a Pannoramic Scan 150 scanner. As previously described, IHC staining and staining score were carried out.[30] Table S2 provides information on primary antibodies.

Lentiviruses and plasmids

In this study, knockdown lentiviruses were generated to express two types of small hairpin RNA (shRNA): negative control shRNA (si-NC) and shRNA targeting SRSF1 utilizing the hU6-MCS-CBh-IRES-puromycin vector. The lentiviruses were then packaged in 293T cells. GeneChem (Shanghai, China) developed and packaged overexpression lentiviruses expressing SRSF1 (LV-SRSF1) and control lentiviruses (LV-Con). Lentiviral vectors were employed to transfect various OSCC cell lines, with an MOI of approximately 10, for a duration of 16 h, utilizing polybrene at a concentration of 6 μg/mL. Consequently, stable cell pool selection was performed 48 h post-infection using puromycin at a concentration of 2.5 μg/mL. As described previously, stable upregulation and downregulation cell lines were established.[31] Transcription factor EB (TFEB) cDNA was synthesized and later subcloned into pcDNA3.1 (GeneChem). pcDNA3.1-TFEB transfection with Lipofectamine® 3000 (Invitrogen, USA) was used to obtain different OSCC cell lines with ectopic TFEB expressions. The empty pcDNA vector was the negative control. Tables S3 and S4 shows their sequences.

Assessment of cell growth, proliferation, and survival

The assessment of cell growth was conducted using the cell counting kit-8 (CCK8) assay in accordance with the directions provided by the producer.[30] Briefly, 5×10^3 cells/well were seeded in a 96-well flat-bottomed plate, grown at 37 °C for 1, 2, 3, 4 or 5 day. After 10 μL WST-8 dye was add to each well, cells were incubated at 37°C for 2 h and the absorbance was finally determined at 450 nm using a microplate reader. Moreover, 5-ethynyl-2′-deoxyuridine (EdU) staining was used to label cell proliferation.[31] A total of 4×10^5 cells were seeded in 6-well plates, which contained coverslips. 24 h later, EdU regent was added into each well and incubated at 37°C for 4-6 h. After washing with PBS and fixing with 4% paraformaldehyde, the coverslips were incubated with 0.3% Triton X-100 and stained with Click Addictive Solution. Finally, the cells were stained DAPI. Anchorage-dependent growth capacities, or cell survival, were assessed using the colony formation assay. Concisely, the cells were grown under controlled temperature and humidity conditions in an incubator with a 5% concentration of CO_2. The temperature was set to 37°C. Subsequently, cells were subjected to formaldehyde fixation, crystal violet staining, photographic documentation, and quantification after ten days.

RNA-seq and data analysis

RNA-sequencing of the stable si-NC and si-SRSF1 groups of SCC-4 and CAL-27 cells was carried out by GeneChem. The mRNA samples were collected, processed, and prepared for library creation following the producer's guidelines. In summary, total mRNA was obtained, and the Qubit RNA Assay Kit in a Qubit 2.0 fluorometer was utilized to determine the RNA concentration. Subsequently, NEBNext UltraTM RNA Library Prep Kit for Illumina was employed to produce sequence libraries following the manufacturer's recommendations. DESeq2 R package (1.16.1) was used to analyze the expression differences between si-NC and si-SRSF1 cells. The threshold levels were log2 (fold change) >1.5 and $q<0.05$.

Lysosomal enzyme assay

The lysosomal cathepsin D (CTSD) and alpha-N-acetylglucosaminidase (NAGLU) activities were measured using the fluorometric CTSD assay kit from Biovision Inc. (K143-100) and the Sigma-Aldrich (CS0780) NAGLU assay kit, respectively, in accordance with the manufacturer's instructions. Quantification of enzyme activities in the entire cell was detected by calculating the alteration in absorbance per μg of protein.

Lysosomal staining

The quantification of the lysosomes was performed using Lyso-Tracker. Lyso-Tracker Red DND-99 (C1046) was purchased through Beyotime Biotechnology (Shanghai, China). Cells were washed and labeled with Lyso-tracker Red. After 30 min, the cells were washed three times with serum-free medium (without phenol red). A subset of cells was chosen as representatives and imaged using a laser confocal microscope to observe the fluorescence intensity.

Ad-mCherry-GFP-LC3 infection analysis

Autophagic flux was monitored by Ad-mCherry-GFP-LC3. Briefly, we seeded cells (5×10^5 cells/well) in a six-well plate, infected them with Ad-mCherry-GFP-LC3 (40 MOI), and cultured them for another 24 h period. After washing with PBS (pH 7.4) until the residues were no longer detectable, the cells were characterized by laser confocal microscopy.

Immunofluorescence

Cells were plated on glass coverslips in 24-well plates. After treatment, the cells were fixed with 4% paraformaldehyde in PBS for 30 min. After washing with PBS, the cells were permeabilized with 0.4% Triton X-100 and blocked with 5% goat serum for 30 min. The indicated primary antibodies were incubated with the cells overnight at 4°C, followed by incubation with secondary antibodies (Abcam 488-conjugated AffiniPure goat anti-mouse IgG (H + L) or Abclonal 594-conjugated goat anti-rabbit IgG (H + L)) at 37°C for 1 h. Images were taken using laser confocal microscopy as soon as possible.

QUANTIFICATION AND STATISTICAL ANALYSIS

Statistical analyses were conducted utilizing the SPSS V19.0 program. Our findings were expressed as mean ± SD for a minimum of n=3. T-tests and one-way ANOVAs were used to compare means between and among groups. To assess the associations between SRSF1 expression patterns and clinic-pathologic characteristics, statistical tests such as the χ^2, Fisher's exact, and student's t-tests were employed. Survival was evaluated employing the Kaplan-Meier approach, and the comparison of curves was performed utilizing the log-rank test. $P<0.05$ was considered significant.